JOURNAL OF MATERIALS SCIENCE **37** (2002) 1083–1090

# Preliminary study of the inhomogeneous precipitate distributions in Nb-microalloyed plate steels

C. L. DAVIS*, M. STRANGWOOD
*The University of Birmingham, School of Metallurgy and Materials, Elms Road, Edgbaston, Birmingham, B15 2TT UK*
*E-mail: c.l.davis@bham.ac.uk*

Three as-thermomechanically controlled rolled (TMCR) microalloyed steels containing Nb levels between 0.023 and 0.057 wt% have been characterised in terms of phase balance and ferrite grain size distribution (optical microscopy and image analysis). In addition, transmission electron microscopy (TEM) has been carried out on carbon extraction replicas from sub-surface and mid-thickness positions to determine fine precipitate size distribution and areal number density in ferrite and pearlite. Precipitate distributions were also determined after simulated re-heating schedules. The ferrite grain size distributions have been related to precipitate distributions and rolling schedules, whilst the development of precipitate distributions has been considered based on solidification, reheating and deformation behaviour. 

## 1. Introduction

High strength low alloy (HSLA) steels have additions of small amounts of titanium, niobium and/or vanadium, which are strong carbide and nitride forming elements, to allow higher strength levels to be achieved with lower carbon contents, without a loss in toughness, weldability or formability [1, 2]. The microalloyed HSLA steels benefit from an improvement in both strength and toughness through the generation of a fine ferrite grain size with additional strengthening being provided by the fine scale precipitation of microalloy carbonitride particles [3]. Niobium is reported to be the most effective microalloying element to achieve refinement of the final grain structure [4]. Precipitates, formed during solidification as the steel is continuously cast, dissolve either fully or partially during slab re-heating. Grain growth will occur during re-heating and will be affected by the presence of pinning particles, so localised partial dissolution may lead to inhomogeneous grain growth. Re-precipitation of Nb-rich particles takes place during and subsequent to rolling, modifies the microstructure and provides the improvement in properties. However, it has been found that some Nb and Nb-V microalloyed plate steel can exhibit a variation in grain size, particularly in the plate sub-surface region. This is typified by a banded ferrite/pearlite morphology with abnormally large ferrite grains in a matrix of smaller grains. These inhomogeneous structures result in variations in mechanical properties, particularly impact toughness, which are undesirable [5].

The grain boundary pinning effect of niobium precipitates during controlled rolling below 1000°C prevents dynamic recrystallisation and retards static recrystallisation [6–8] thus affecting the final ferrite grain size. Niobium is known to partition to the interdendritic regions during solidification and also to promote the partitioning of other elements such as carbon and nitrogen [9, 10]. Any partitioning of niobium will affect the local Nb concentration in solution and hence the subsequent nucleation behaviour and final volume fraction of Nb-rich precipitates. This inhomogeneous precipitate distribution may affect the local recrystallisation and recovery processes and hence the final ferrite grain size. In addition, the precipitation of Nb(C,N) in the solid state proceeds very slowly when the material is unstrained, even during isothermal holding at temperatures as high as 900°C. However, upon deformation of the austenite this process speeds up considerably indicating that the nucleation rate of Nb(C,N) precipitates is strain dependent [11]. Thus there may also be an influence of rolling history, i.e. deformation levels, on the final ferrite grain structure.

The aim of this paper is to characterise the precipitate distribution in steels containing a range of Nb-levels and to determine if there is a link between precipitate distribution, rolling deformation and ferrite grain size.

## 2. Experimental procedure

Three continuously cast and hot rolled samples were supplied by Corus, which represented principally differences in niobium level, Table I, between 0.023 and 0.057 wt%. There were also variations in C level (steel 3 having about half that in steels 1 and 2) and minor differences in Mn, Si, P, Al and Ti levels. The differences

*Author to whom all correspondence should be addressed.

TABLE I Compositions of the steels used (wt%)

| | C | Mn | Si | P | S | Al | N | **Nb** | V | Ti |
|---|---|---|---|---|---|---|---|---|---|---|
| Steel 1 | 0.09 | 1.44 | 0.36 | 0.010 | 0.003 | 0.041 | 0.006 | **0.023** | 0.004 | 0.006 |
| Steel 2 | 0.11 | 1.39 | 0.34 | 0.016 | 0.003 | 0.027 | 0.005 | **0.032** | 0.003 | 0.003 |
| Steel 3 | 0.05 | 1.53 | 0.26 | 0.010 | 0.001 | 0.047 | 0.005 | **0.057** | 0.003 | 0.007 |

TABLE II Rolling schedule temperature data for steels 1, 2 and 3

| | Steel 1 | Steel 2 | Steel 3 |
|---|---|---|---|
| Reheat temperature (°C) | 1150 | 1200 | 1150 |
| Start hold temperature (°C) | 1025 | 926 | 995 |
| Finish hold temperature (°C) | 820 | 817 | 820 |
| Finish roll temperature (FRT) (°C) | 749 | 691 | 748 |

in composition on solidification sequence and equilibrium structures during cooling were rationalised using thermodynamic predictions using Thermo-Calc version N. This has been shown to be valid for coarse, liquid-formed precipitates and to account (at least qualitatively) for finer scale, solid-state carbo-nitride precipitation [12]. The slabs were reheated to 1200°C with steel 2 being rolled to its final thickness (single reheat), whilst steels 1 and 3 were part rolled to 150 mm thickness at a Corus commercial plate mill. Steels 1 and 3 were later reheated (to 1150°C) and finish rolled on an experimental mill at the Corus Swinden Technology Centre. The rolling schedules, in terms of gauge reduction and % reduction, for the three steels are shown in Fig. 1 and the temperature data are shown in Table II. Steels 1 and 3 received the same thermo-mechanically controlled rolling (TMCR) schedule with the hold occurring after pass 5 whereas steel 2 received a different TMCR schedule with the hold occurring after pass 8.

Full thickness slices were taken from the centre of each plate width; mounted in conducting bakelite, ground and polished to a 0.25 $\mu$m $Al_2O_3$ paste finish prior to etching in 2% nital. The microstructure was characterised at the sub-surface, quarter-thickness and mid-thickness positions in terms of ferrite grain size distribution (based on a minimum of 1000 grains for each condition) and the percentage of second phase measured from optical specimens on a Quantimet 500 image analyser. Carbon extraction replicas were taken from the sub-surface and mid-thickness position and examined using a Philips CM20 transmission electron microscope (TEM) operating at 200 kV. It should be noted that carbon extraction replicas have been found not to reveal very fine (<5 nm) particles [13]. A minimum of 1000 particles was measured for each condition. The TEM was fitted with a LINK QX2000 energy dispersive X-ray spectroscopy (EDS) system and selected particles were analysed by EDS to determine the substitutional alloying elements present with crystal structure being determined by selected area diffraction pattern (SADP) analysis.

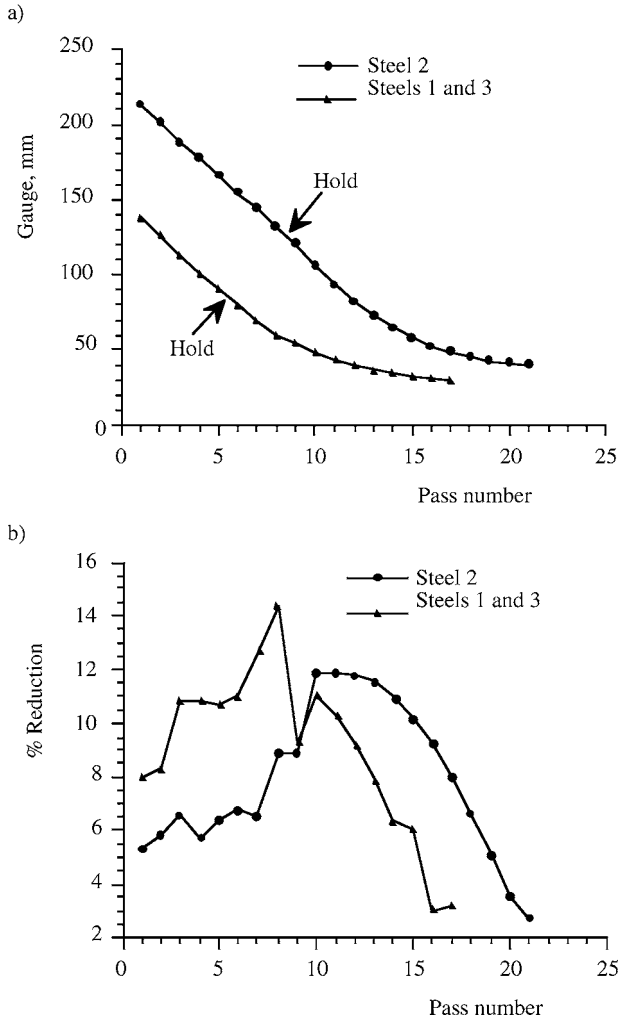


*Figure 1* Rolling schedules showing (a) gauge reduction and (b) % reduction.

## 3. Results and discussion

### 3.1. Thermodynamic calculations

The lower carbon content of steel 3 results in equilibrium solidification completely as $\delta$-ferrite rather than as primary $\delta$-ferrite followed by a mixture of austenite and $\delta$-ferrite as predicted for steels 1 and 2, Table III. However, the effects of non-equilibrium cooling rates would be to change the solidification mode from primary $\delta$-ferrite to mixed austenite and $\delta$-ferrite in steel 3 and reduce primary $\delta$-ferrite to less than the predicted 85% in steels 1 and 2 i.e. cause the change in solidification structure to occur closer to the slab surface than predicted [14, 15]. Table III also shows the maximum temperature at which the Nb-rich precipitate phase is stable in these steels. Whilst TiN and MnS are expected to start forming just below the completion of solidification so that very coarse particles are not expected, those that form should remain during and after any reheating stages. The volume fractions of these precipitates are predicted to be about one third to one quarter that expected for Nb(C,N)-based precipitates formed between the temperatures given in Table III and the start

TABLE III Thermo-Calc predictions for the solidification and precipitation sequence in steels 1, 2 and 3

| | Steel 1 | Steel 2 | Steel 3 |
|---|---|---|---|
| Solidification sequence | $L \rightarrow L+\delta \rightarrow L+\delta+\gamma \rightarrow \delta+\gamma$ | | $L \rightarrow L+\delta \rightarrow \delta$ |
| Nb(C,N) solution temperature, °C | 1104 | 1162 | 1114 |

of $\alpha$-ferrite formation on cooling. For all three steels, reheating is carried out above the Nb(C,N) dissolution temperature and all Nb-rich precipitates should have been taken back into solution prior to rolling. Rolling, before the TMCR hold period, occurs in the Nb(C,N) precipitation temperature range for all three steels, the extent of this being greatest for steel 2 (≈240°C) and much smaller for the other two steels (120°C for steel 3 and 75°C for steel 1). The finish roll temperature for all three steels is in the austenite and $\alpha$-ferrite two phase field when the majority of Nb(C,N) precipitation should be complete.

## 3.2. Matrix microstructure

All three steels exhibit a microstructure of ferrite and pearlite banded in the rolling direction; steel 3 shows a smaller volume fraction of pearlite consistent with its lower carbon content. In general, steels 1 and 3 show a more equiaxed ferrite grain morphology than steel 2 which may be a consequence of their higher FRTs (Table II). Steel 2, however, shows a more elongated ferrite grain morphology and also bands of coarse ferrite grains resulting in 'streaking' on a macro sample at the sub-surface location as shown in Fig. 2. Fig. 3 gives higher magnification micrographs of the sub-surface, quarter-thickness and mid-thickness positions for steel 2 as well as the sub-surface region for steels 1 and 3 for comparison. The sub-surface micrograph of steel 2, Fig. 3c, clearly shows the presence of coarse ferrite grains in a band sandwiched by bands of much finer ferrite grains resulting in a 'duplex' ferrite grain size distribution. The presence of very fine ferrite grains to a depth of over 300 $\mu$m below the plate surface could be due to the low finish rolling temperature (691°C) and small final gauge reductions experienced by the plate resulting in preferential surface deformation. This, however, would not account for the band of coarse ferrite grains observed in the middle of these fine bands. The rolling schedule for steels 1 and 3 does not give such fine grained structures, Fig. 3a and b, and, although inhomogeneities in ferrite grain size are observed, there are no clear bands of coarse and fine grained ferrite as seen for steel 2. The quarter-thickness position, Fig. 3d, shows the presence of fine and coarse ferrite grains but the difference in size is less pronounced than at the sub-surface position, but is still greater than that at the sub-surface locations in steels 1 and 3. The quarter-thickness position should be less affected by low FRT and small gauge reductions than the sub-surface positions. The mid-thickness position, Fig. 3e, shows relatively coarse ferrite grains, although some finer ferrite grains can also be seen, with a less distinct 'duplex' grain size distribution. The ferrite grains at the mid-thickness position tend to be more equiaxed than at the sub-surface and quarter-thickness positions.

The equiaxed ferrite grain morphology for steels 1 and 3 allowed the equivalent circle diameter to be used as a measure of grain size, whereas the ferrite grains in steel 2 are elongated in the rolling direction and so grain breadth values were determined using the linear intercept method to quantify the grain structure. Grain size distributions were determined at all three positions for steel 2 and are presented in Fig. 4. In steels 1 and 3 the differences in distribution between locations and between steels were much less significant and so only

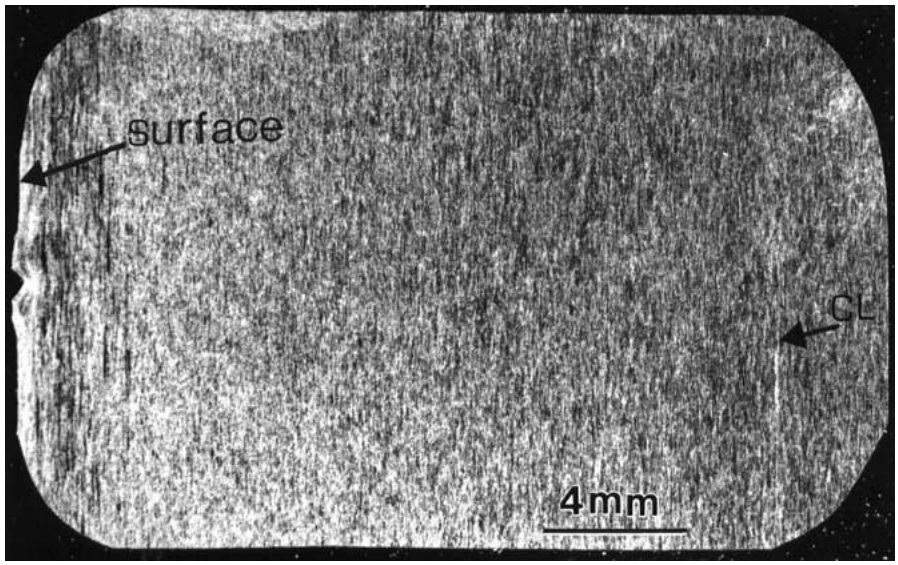


*Figure 2* Optical micrograph through thickness for steel 2 showing the plate centre line (CL) and 'streaking' caused by the large grains in the sub-surface region.

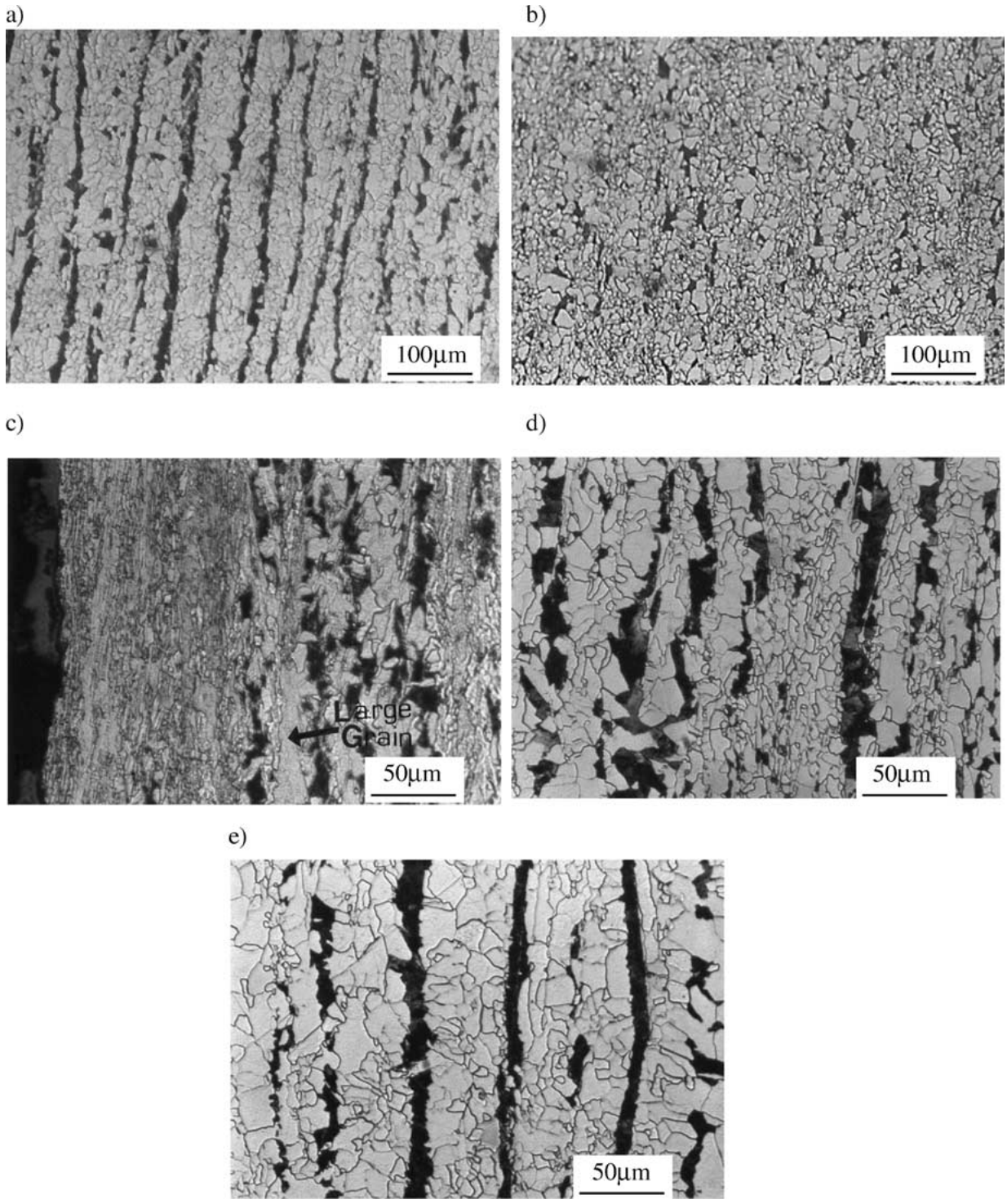


*Figure 3* Optical micrographs showing the sub-surface position for (a) steel 1 and (b) steel 3 and for steel 2 showing (c) sub-surface (d) quarter thickness and (e) mid-thickness positions.

the sub-surface and mid-thickness distributions are presented for steel 1 in Fig. 5. The distributions in Fig. 4 quantify the trends seen in Fig. 3 in that the most frequent grain breadth increases from sub-surface through quarter thickness to mid-thickness and that the proportion of fine ferrite grains ($<6\ \mu$m) is much greater in the sub-surface position than in either of the other two positions. However, the proportion of coarse ferrite grain breadths ($>7\ \mu$m) is similar for all three positions with the largest grain being recorded in the sub-surface position. Hence the grain size distributions show a more 'duplex' grain size for the sub-surface position. The grain size distributions for steels 1 and 3 are similar for sub-surface and mid-thickness locations, Fig. 5, and do not show the same duplex grain size distribution exhibited in the sub-surface regions of steel 2. The duplex grain structure means that the quoting of an average grain size for the sub-surface region of steel 2 has little relevance. For more homogeneous distributions (mid-thickness of steel 2; sub-surface and mid-thickness of steels 1 and 3) then average grain sizes are more meaningful and they show trends of increasing with depth and decreasing with Nb content (and hence predicted volume fraction of Nb(C,N)), Table IV.

TABLE IV Mean ferrite grain size and standard deviations ($\mu$m)

| Steel | Sub-surface | Mid-thickness |
|---|---|---|
| 1 | $5.3 \pm 3.9$ | $6.3 \pm 4.8$ |
| 2 | NA | $6.0 \pm 3.5$ |
| 3 | $4.8 \pm 2.9$ | $5.1 \pm 3.5$ |

NA – not applicable.

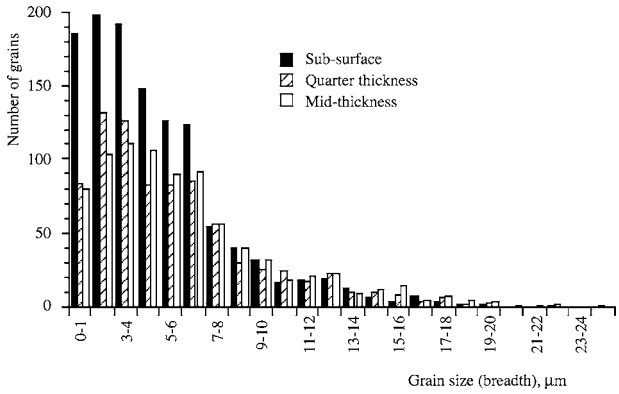


*Figure 4* Grain size (breadth) distribution curve for the sub-surface, quarter thickness and mid-thickness positions in steel 2.

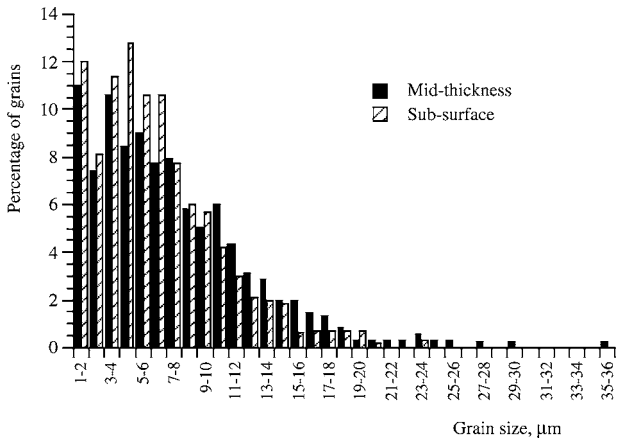


*Figure 5* Grain size (equivalent diameter) distribution curve for the sub-surface and mid-thickness positions in steel 1.

## 3.3. Fine scale precipitation

TEM analysis of carbon extraction replicas from the sub-surface regions of all three steels in the as-rolled condition were analysed in order to quantify precipitate populations for both ferrite and pearlite phases. For steels 1 and 2 the volume fraction of pearlite varied between 10 and 12.5%, whereas the lower carbon content of steel 3 gave a smaller volume fraction of 4–6%. The particles detected by TEM had a fcc structure (from SADP analysis) and EDS revealed high levels of Ti and/or Nb indicating that they are based on (Ti,Nb)(C,N). The results are summarised in Table V in terms of average particle size (diameter or side length depending on morphology) and areal number density. The latter quantity was used as no accurate determinations of replica thickness were made to calculate volume number density; this will result in some variation in values but they can still be used as a qualitative measure to indicate trends in particle number densities. An increase in the overall Nb level is associated with a decrease in the average size of precipitates but an increase in areal number density in the ferrite phase. This trend may also be affected by the lower C content of steel 3 and differences in processing. The situation in pearlite is less clear although a larger average precipitate size is associated with a lower areal number density. The variation in average precipitate size with Nb content shows an initial increase from steel 1 to 2 followed by a decrease from steel 2 to 3. This means that, for steel 1, the average particle size in ferrite is the same as in pearlite with a higher number density in the latter, but, in steels 2 and 3, the average size in pearlite is greater than in ferrite with a lower number density. The particle sizes showed a broader more normal distribution in pearlite than in ferrite, which tended to have a more narrow distribution skewed to larger sizes, as shown by the example of steel 2, Fig. 6. The combination of size and areal number density results in a greater volume fraction of precipitates in pearlite for all three steels.

TABLE V Precipitate sizes, number densities and volume fractions for the sub-surface positions in steels 1, 2 and 3

| | Average ppt. size, nm | | Number density, ($\times 10^{-6}$) ppmm$^{-2}$ | |
|---|---|---|---|---|
| | Ferrite | Pearlite | Ferrite | Pearlite |
| Steel 1 | 36 | 36 | 9.6 | 21.6 |
| Steel 2 | 21 | 57 | 11.3 | 7.6 |
| Steel 3 | 15 | 28 | 43.6 | 33.2 |

Precipitate populations have previously [16, 17] been investigated for steels 1 and 3 for hot rolling (HR) and interpass cooling (IPC) processing routes which indicated the same behaviour for precipitates in steel 1 as reported here for TMCR processing. For steel 3, however, the average precipitate size was greater in pearlite than in ferrite for all processing but differences in areal number density were noted. IPC and TMCR processing had a significantly higher number density of particles in ferrite rather than in pearlite whilst for the HR condition a slightly greater number density was seen in pearlite.

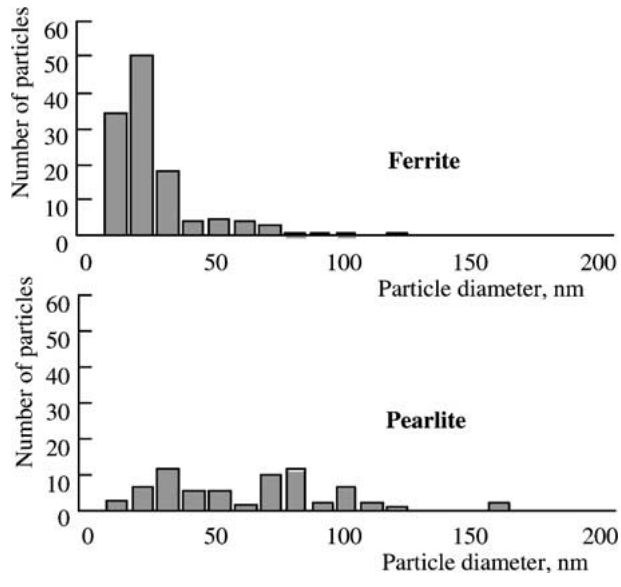


*Figure 6* Precipitate distributions determined from approximately equal areas at the sub-surface position in the ferrite and pearlite regions of steel 2.

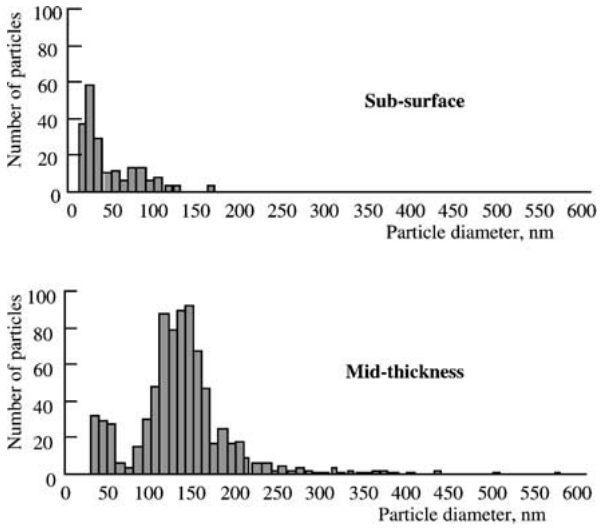


*Figure 7* Precipitate distributions determined from approximately equal areas at the sub-surface and mid-thickness positions in steel 2.

Precipitate distributions will develop during all stages of processing, i.e. from initial casting through reheating and rolling. Hence there may be spatial variations, through the slab/plate thickness, in the populations of Nb(C,N) particles, as well as local variations in populations between phases (ferrite and pearlite), and so distributions were also determined at the sub-surface and mid-thickness positions for steel 2; these results are shown in Fig. 7. The size range and average size of precipitates in the mid-thickness position both increased compared with the sub-surface position, which, along with a much larger areal number density resulted in a greater volume fraction. This spatial variation is likely to be dominated by segregation during casting.

The effects of reheating were investigated by repeating the reheating schedule on rolled plate and water quenching. Ti(C,N), which has a higher solution temperature than Nb(C,N), would be expected to remain after reheating to 1150°C or 1200°C and TEM analysis of extraction replicas from the sub-surface regions of steel 1 samples reheated to the solution temperature (1150°C) showed that only Ti-based cuboidal precipitates were present at a smaller size and much smaller areal number density than in the rolled material. Equivalent samples from steels 2 and 3 also showed a reduction in size and number density of precipitates with the majority of these being cuboidal Ti-rich particles, Fig. 8a. However, occasional rounded Nb-rich precipitates were also present, often as caps on cuboidal particles, Fig. 8b. Hence, it is suggested that the solution temperatures and times for steels 2 and 3 were not sufficient to fully dissolve the Nb-rich precipitates despite the reheat temperatures being approximately 40°C above the predicted Nb(C,N) solution temperature. This is due to the increased size of the precipitates in the prior pearlite regions not fully dissolving during the reheat time. In addition segregation of Nb to these regions will increase the local solution temperature.

### 3.4. Precipitate development

The precipitate population will initially form during the relatively slow solidification, and hence low cooling rates, associated with continuous cooling. The slabs of all steels will start to solidify as $\delta$-ferrite and, as cooling rates are not slow enough to be equilibrium, will at some depth change to solidification as both $\delta$-ferrite and austenite. This will occur even for steel 3 but much nearer to the centreline (mid-thickness) than for steels 1 and 2. Associated with this solidification process will be solute segregation; both macro- and micro-segregation [18]. Thus, the initial metal to solidify will do so as Nb-depleted $\delta$-ferrite at the interface with the water-cooled copper mould. This region will be associated with the surface and sub-surface regions of the rolled plate. Solidification at the sub-surface region will be completed as $\delta$-ferrite so that micro-segregation of elements such as Nb to interdendritic or cellular boundary areas will coincide with $\delta/\delta$ grain boundaries. Full transformation from $\delta$-ferrite to austenite is expected prior to precipitation of Ti- and Nb-rich phases and so the centres of the austenite grains will correspond to the solute-enriched regions whilst $\gamma/\gamma$ grain boundaries will be solute-depleted. As cooling proceeds the higher solute content in the austenite grain centres will result in a greater driving force for precipitation and so formation at higher temperatures leading to greater time for growth and a higher volume fraction due to the greater amount of solute. The number density of particles will depend on nucleation rate

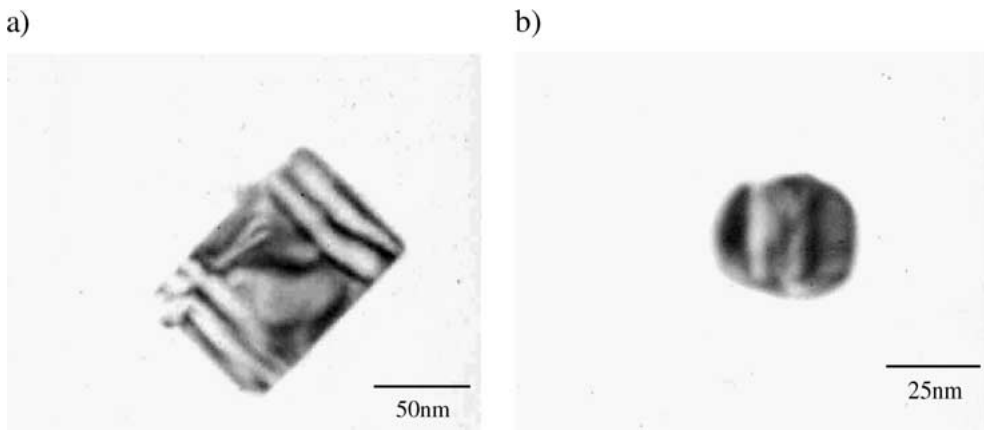


*Figure 8* TEM micrographs showing (a) a cuboidal TiN precipitate in steel 1 and (b) a mixed (Ti,Nb)(C,N) particle in steel 3 after the simulated reheat.

and so the precise relationship between cooling rate and continuous-cooling-transformation (CCT) curve. Hence it is expected that there will be a greater Nb(C,N) precipitate size and number density in pearlite since the $\gamma/\gamma$ grain boundaries will tend to transform to $\alpha$ and the centre of the $\gamma$ grains will form pearlite.

Moving further into the cast slab the overall Nb and Ti levels increase leading to greater volume fractions and sizes of precipitates, as seen in Fig. 7. At the depth at which the solidification sequence changes then micro-segregation would take place to $\delta/\gamma$ boundaries so that the resulting solute rich regions can occur at $\gamma/\gamma$ boundaries and in the $\gamma$ grain centres. Hence a more even distribution of precipitates between ferrite and pearlite would be expected at the mid-thickness position.

Reheating after casting should fully re-dissolve the Nb-rich precipitates, particularly in the sub-surface regions where macro-segregation results in lower overall solute levels. Re-solution treatments in this work showed that the reheating schedule adopted for steel 1, with the lowest Nb level, was sufficient to fully re-dissolve these particles, but not the Ti-rich cuboidal particles. In steels 2 and 3 the reheating time and/or temperature were not sufficient to fully dissolve Nb-rich particles so that some remain prior to rolling with the proportion expected to increase towards the centreline.

Reprecipitation of Nb-rich carbonitrides will occur during TMCR processing, starting at the initial stages of rolling when large deformation roughing passes are applied. In this temperature range particles of the order of 10 nm have been shown to form [13]. Further precipitation occurs during the hold period which takes place between about 1025°C and 820°C. The size, volume fraction and number density of precipitates formed in this temperature range depend on a variety of factors including local composition and nucleation site density. For the Nb composition range in these steels the nose of the precipitation-temperature-time C-curve where nucleation of precipitates is most rapid corresponds to the hold temperature range [19]. Therefore, during the hold there is a high thermodynamic driving force for precipitation and sufficient time to allow diffusion to suitable nucleation sites. Previous work suggests that there is little growth of these particles during the hold period since they are close to the size of those observed following hot rolling and interpass cooling schedules where the hold is absent [16, 17]. Once rolling recommences below 820°C further strain induced precipitation can occur.

During the hold the temperature decreases to below the predicted recrystallisation stop temperature (the lowest recrystallisation stop temperature will be for the lowest Nb content steel, steel 1, and is 940°C [20]) such that when rolling recommences an elongated austenite grain structure is produced. This 'pancake' structure has a high surface area to volume ratio and, since recrystallisation is not taking place and recovery is limited, there is also a build up of dislocations within the grains. The pancake structure provides a large number of transformation nucleation sites and consequently the final microstructure contains fine, equiaxed ferrite grains.

However, the predicted recrystallisation stop temperature assumes a homogenous microstructure, including microalloying elements in solution and as precipitates. The results above indicate that the Nb-microalloyed steels used in this investigation do not have a homogenous microalloy distribution. The results presented in Table V and Fig. 6 show that there are differences in the microalloy precipitate size and number density between the ferrite and pearlite regions in the three steels. The precipitates tend to be smaller in ferrite than in pearlite and generally there is a higher number density of precipitates in the ferrite (except for steel 1). It has also been seen that there is consistently a higher volume fraction of precipitates in the pearlite phase compared to the ferrite phase, although there are differences in the number densities present. The inhomogeneous precipitate distribution occurs because Nb (as well as Ti, C and N) segregate to the liquid phase during solidification as discussed above. TEM precipitate analysis of the rolled steels supports the suggestion that segregation during solidification results in an inhomogeneous microalloying element concentration and consequently microalloying precipitate volume fraction in the steel, with an increased volume fraction being observed in pearlite as predicted.

The resulting inhomogeneous precipitate distribution in the Nb-containing steels will influence microstructural development during rolling. If there is an inhomogeneous precipitate distribution in the steel then there will not necessarily be complete recrystallisation or the same extent of grain growth in all parts of the steel at the same time since the presence of fine precipitates pins grain boundaries and retards the recrystallisation process. There will be a complex interaction between the precipitate distribution and the strains introduced during rolling that control the extent of recovery and recrystallisation and hence the final ferrite grain size distribution. This gives some degree of grain inhomogeneity in steels 1 and 3 but this is much more severe in steel 2.

Steels 1 and 3 received the same rolling schedule, Fig. 1. Both steels show a similar grain size distribution with relatively equiaxed ferrite grains being observed at the sub-surface and mid-thickness positions. Steel 3 has a finer ferrite grain size at both the sub-surface and mid-thickness positions compared to steel 1 which correlates with the increase in number density (and volume fraction) of microalloy precipitates present in steel 3 due to its higher Nb content. The Nb-rich precipitates will tend to form at a higher temperature in steel 3 due to the increased driving force for nucleation resulting from the increased Nb content in the steel. This, along with the increased number (and reduced average size) of precipitates, reduces the recrystallisation stop temperature during processing increasing the amount of deformation retained in the microstructure and hence the degree of 'pancaking' of the grains. Thus a finer ferrite grain structure develops on transformation from the deformed austenite grains. It is suggested that the inhomogeneous distribution of the Nb-rich precipitates in steels 1 and 3 has not resulted in a duplex ferrite grain size being developed because the interaction between

the deformation strains and precipitates did not result in significant localised variations in recrystallisation occurring in the steel. In steel 1 this could arise because of the lower degree of inhomogeneity of precipitates due to the low overall Nb level and so reduced segregation effects. Steel 3 has the highest level of Nb and so should show the greatest segregation effects; however, the ferrite grain size variations would indicate that the interaction of rolling strains and precipitate distribution does not result in duplex grain structures.

Steel 2 has a similar Nb-rich precipitate distribution to steel 3 in terms of the differences in number density and size between the pearlite and ferrite. However, a duplex ferrite grain size distribution is observed in the final rolled microstructure, particularly at the subsurface position. The microstructure in this region of steel 2, Fig. 3c, has banded very fine ferrite grains separated by a band of coarse ferrite and pearlite. The surface duplex structure could arise from more localised strain variations, but this is unlikely to account for the duplex structure at the quarter thickness position, Fig. 3d. The coarser ferrite grains are generally located between closely spaced pearlite bands and so the different distribution of Nb-rich precipitates between ferrite and pearlite noted in this study would be consistent with a reduction of grain boundary pinning in the ferrite between pearlite colonies. The reheating schedule for steel 2 (and steel 3) does not fully re-dissolve Nb-rich precipitates which will remain mostly in pearlite regions. Growth of these precipitates can occur on hot rolling in preference to nucleation of new precipitates which would reduce the number densities in pearlite relative to the ferrite and result in a larger precipitate size in pearlite, as seen in Table V for steels 2 and 3 compared with steel 1. Steel 2 received a different rolling schedule than steels 1 and 3 and it is suggested that localised variations in recrystallisation occurred because of the differences in the effect of grain boundary pinning by the inhomogeneous precipitate distribution at the strain levels experienced.

## 4. Conclusions and further work

Characterisation of the ferrite grain size distributions and the Nb-rich precipitate distributions at the subsurface and mid-thickness plate positions in three niobium-containing HSLA steels processed by different TMCR schedules has shown:

- The volume fraction and average size of Nb-rich particles at the sub-surface position is significantly less than at the mid-thickness position.
- Different precipitate sizes, number densities and volume fractions were observed in the ferrite and pearlite regions in the final rolled steel microstructures. A greater volume fraction of Nb-rich precipitates was observed in the pearlite compared to the ferrite however the precipitates in the ferrite were generally smaller. The distributions are consistent with segregation of Nb (and Ti) during solidification. Verification of the link between precipitate distributions and solidification segregation requires analysis of particle distributions in the as-cast slab, which is underway.
- A duplex ferrite grain size distribution results from the combination of inhomogeneous Nb-rich precipitate distributions in the steel and the rolling schedule used. An inhomogeneous precipitate distribution is not sufficient itself to cause duplex grain size formation. The relationship between particle distributions and ferrite grain size will require confirmation through thin foil TEM, which is also underway.

## Acknowledgements

The financial support of the Engineering and Physical Sciences Research Council (EPSRC) and the Corus Group (formerly British Steel plc.) are gratefully acknowledged. The research of Suzanne Williams and Diane Talbot are acknowledged in the preparation of this paper. Thanks are due to Professor I. R. Harris for the provision of research facilities at the University of Birmingham.

## References

1. A. J. DEARDO, in Proc. of 2nd Int. Conf. on HSLA Steels, Beijing, China, edited by G. Tither and S. Zhang (TMS, 1992) p. 21.
2. G. TITHER, in Proc. of 2nd Int. Conf. on HSLA Steels, Beijing, China, edited by G. Tither and S. Zhang (TMS, 1992) p. 61.
3. L. VOLLRATH and KH. G. SCHMITT-THOMAS, in Proc. of Conf. HSLA Steels-Metallurgy and Applications, Beijing, China (ASM Intl, 1986) p. 599.
4. A. C. KNESSI, G. POSCH, C. I. GARCIA and A. J. DEARDO, in Proc. of Intl. Symp. on Low-Carbon Steels for the 90's, Pittsburgh, USA, edited by R. Asfahani and G. Tither (TMS 1993) p. 113.
5. F. MAAS, Corus Internal Report.
6. J. A. RODRIGUES and J. R. DERMONDE, *Mat. Sci. and Tech.* (1985) 29.
7. I. TAMURA, C. OUCHI, T. TANAKA and H. SEKINE, "Thermo-Mechanical Processing of HSLA Steels" (Butterworths, Stoneham, MA 1988).
8. J. R. WILCOX and R. W. K. HONEYCOMBE, *Mat. Sci. and Tech.* **3** (1987) 849.
9. G. TITHER and Z. SHAUHAU, The Minerals, Metals and Materials Society (1992) p. 115.
10. Z. CHEN, M. H. LORETTO and R. C. COCHRANE, *Mat. Sci. and Tech.* **3** (1987) 836.
11. M. J. LUTON, R. DARVEL and R. A. PETKOVIC, *Metall. Trans.* (1980) 411.
12. J. E. BERRY, J. Z. MORRIS, C. L. DAVIS and M. STRANGWOOD, in 32nd Annual IMS Convention, Cincinnati, USA, November 1999 (Pub ASM Intl 1999).
13. B. DUTTA and C. M. SELLARS, *Mat. Sci. and Tech.* **2** (1986) 146.
14. H. FREDRICKSSON, *Metall. Trans.* **3** (1972) 2989.
15. *Idem.*, *Scad. J. Metall*. **5** (1976) 27.
16. D. TALBOT, C. L. DAVIS and M. STRANGWOOD, in 32nd Annual IMS Convention, Cincinnati, USA, November 1999 (Pub ASM Intl, 1999).
17. *Idem.*, in Int. Conf. on 'Thermomechanical Processing of Steels,' London, UK, May 2000 (IoM, London, 2000).
18. M. WOLF, in 3rd International Conference on Solidification Processing (1987) p. 182.
19. A. J. ROSE and A. A. HOWE, Corus Internal Report.
20. E. J. PALMIERE, C. I. GARCIA and A. J. DEARDO, *Metall. Trans.* **27A** (1996) 951.

*Received 29 June*
*and accepted 2 November 2001*